(RESEARCH ARTICLE)

Effect of nonlinear thermal radiation on second order slip flow and heat transfer of Jeffrey nanofluid over a stretching sheet with non-uniform heat source/sink

P. Ashok [1], Ch. Vittal [2], Vijayalaxmi Tankasala [3, *], M. Chennakrishna Reddy [1] and S.Renuka [4]

[1] Department of Mathematics, University College of Science, Osmania University, Hyderabad-500007, India.
[2] Department of Mathematics, University College of Science, Saifabad, Osmania University, Hyderabad-500007, India.
[3] Department of Mathematics, NTR GDC (W), Mahabubnagar-509001, Telangana, India.
[4] Department of Mathematics, Nizam College, Osmania University, Hyderabad-500007, India.

Abstract

The flow and heat transfer of Jeffrey nanofluid over a stretching sheet with non-uniform heat source/sink is considered in the present analysis. Effects of nonlinear thermal radiation and second order slip are taken along with uniform magnetic field. System of partial differential equations governing the described problem is reduced to nonlinear ordinary differential equations with aid of similarity transformations. Further, reduced equations are solved numerically using Runge-Kutta-Fehlberg 45 order method with shooting technique. Effects all flow pertinent parameters are recorded in terms of tables and graphs. The results are studied with help of plotted graphs, tables. Results are compared with existing one for some limiting cases and are found to be excellent agreement. It is found that both first, second order velocity slip parameters reduces the thickness of momentum boundary layer and hence decrease the velocity as a result of this one can find the increase in thermal boundary layer.

Keywords: Nonlinear thermal radiation; Second order slip flow; Jeffrey nanofluid; Stretching sheet; Non-uniform heat source/sink; Numerical solution.

1. Introduction

Boundary layer flow over a stretching surface with velocity slip and temperature-jump boundary conditions is an important type of flow and heat transfer occurring in several engineering applications. In these types of transport phenomena, the equations corresponding to continuum equations of momentum and energy are still governed by the Navier-Stokes equations, but the effects of the walls are taken into account by using appropriate boundary conditions. No-slip condition is inadequate for most non-Newtonian liquids, as some polymer melt often shows microscopic wall slip and that has a controlling influence by a nonlinear and monotone relation between the slip velocity and the traction. It is known that, a viscous fluid normally sticks to boundary and there is no slip of the fluid relative to the boundary. However, in some situations there may be a partial slip between the fluid and the boundary. For such fluid, the motion is still governed by the Navier Stokes equations, but the usual no-slip condition at the boundary is replaced by the slip condition. Partial velocity slip may occur on the stretching boundary when the fluid is particulate such as emulsions, suspensions, foams and polymer solutions. In various industrial processes, slip effects can arise at the boundary of the pipes, walls, curved surfaces etc. A boundary layer slip flow problem arises in polishing of artificial heart valves and internal cavities. Recently many authors obtained analytical and numerical solutions for boundary layer flow and heat transfer due to a stretching sheet with slip boundary conditions.

* Corresponding author: Dr. Vijayalaxmi Tankasala; Email:vijaya9966998024@rediffmail.com

Some of the authors have considered second order slip boundary conditions to study the flow, heat and mass transfer by employing boundary layer approximations and seeking similarity solutions [1-5]. Khader [6] obtained numerical solution by Laguerre collocation method to study the effect of viscous dissipation on the steady flow with heat transfer of Newtonian fluid towards a permeable stretching surface embedded in a porous medium with second order slip effect. Abdul Hakeem et al [7] performed both numerical and analytical solution to study the effect of magnetic field on a steady two dimensional laminar radiative flow of an incompressible viscous water based nanofluid over a stretching/shrinking sheet with second order slip boundary condition. Very recently, Mabood and Mastroberardinob [8] considered the second order slip boundary conditions to investigate the effects of viscous dissipation and melting on MHD boundary layer flow of an incompressible, electrically conducting water-based nanofluid over a stretching sheet. Hayat et al [9] studied a steady three-dimensional boundary layer flow of water based nanofluid with copper as nanoparticle over a permeable stretching surface with second order velocity slip and homogeneous–heterogeneous reactions. Zhu et al [10] have investigated the effects of the second-order velocity slip and temperature jump boundary conditions on the magnetohydrodynamic (MHD) flow and heat transfer of water-based nanofluids containing Cu and Al_2O_3 in the presence of thermal radiation. Megahed [11] obtained numerical solution to study the boundary layer flow and heat transfer for an electrically conducting Casson fluid over a permeable stretching surface with second-order slip velocity model and thermal slip conditions in the presence of internal heat generation/absorption and thermal radiation. Further, he has shown that an increase in the velocity and thermal slip parameters results in decrease of the rate of heat transfer.

Heat transfer, influenced by thermal radiation has applications in many technological processes, including nuclear power plants, gas turbines and various propulsion devices for aircraft, missiles, satellites and space vehicles. A linear radiation is not valid for high temperature difference and also dimensionless parameter that is used in the linearized Rosseland approximation is only the effective Prandtl number, whereas in case of non-linear approximation the problem is governed by three parameters, Prandtl number, the radiation parameter and the temperature ratio parameter. First time in the literature, Pantokratoras [12] investigated the effect of linear/nonlinear Rosseland radiation on steady laminar natural convection along a vertical isothermal plate by using a new radiation parameter called film radiation parameter. Hayat et al [9] analysed the effect of nonlinear thermal radiation and constant applied magnetic field on magnetohydrodynamic three-dimensional flow of couple stress nanofluid and viscous nanofluid in the presence of thermophoresis and Brownian motion effects. Shehzad et al [13] have explored the characteristics of thermophoresis and Brownian motion in magnetohydrodynamic three-dimensional flow of nano-Jeffrey fluid in the presence of nonlinear thermal radiation.

In the recent year, non-Newtonian nanofluid has become more and more important due to its enormous industrial applications. Many studies are focused on non-Newtonian fluid as a base fluid with suspended nanoparticles over a stretching sheet. Hayat et al. [14] studied the effects of thermophoresis and Brownian motion on the three-dimensional (3D) boundary layer flow and convective heat transfer of Jeffrey nanofluid over a bi-directional stretching surface with newly developed boundary condition with zero nanoparticles mass flux. Shehzad et al. [15, 16] investigated the effects of convective heat and concentration conditions in magnetohydrodynamic two-dimensional and three-dimensional flow of Jeffrey nanofluid fluid with nanoparticles. Dalira et al. [17] numerically studied the entropy generation for steady laminar two-dimensional forced convection magnetohydrodynamic (MHD) boundary layer flow, heat transfer and mass transfer of an incompressible non-Newtonian nanofluid over a linearly stretching, impermeable and isothermal sheet with viscous dissipation. Abbasi [18] analyzed the influence of heat and mass flux conditions on hydromagnetic steady flow of Jeffrey fluid in the presence of thermal radiation with Brownian motion and thermophoresis effects.

Another important aspect, which influences heat transfer processes, is heat source/sink effect. Many of the authors have studied the heat transfer by considering a uniform and non-uniform heat source/sink effects, which are crucial in controlling the heat transfer. Pal [19] studied the effects of unsteadiness parameter, thermal radiation, suction/injection parameter and non-uniform heat source/sink parameter on flow and heat transfer characteristics of an incompressible viscous fluid over an unsteady stretching permeable surface. Hakeem et al [20] investigated the effect of non-uniform heat source/sink on heat transfer in a Walter's liquid B fluid over an impermeable stretching sheet in the presence of thermal radiation. Manjunatha et al [21] presented numerical results to study the heat transfer analysis of steady two dimensional flow of conducting dusty fluid over a stretching cylinder immersed in a porous media under the influence of non-uniform source/sink. Pal and Chatterjee [22] have carried out a numerical solution to study the effects of viscous-Ohmic dissipation and variable thermal conductivity on steady two-dimensional hydromagnetic flow, heat and mass transfer of a micropolar fluid over a stretching sheet embedded in a non-Darcian porous medium with non-uniform heat source/sink and thermal radiation. Dhanai et al [23] obtained multiple solutions in MHD boundary layer flow and heat transfer of power-law nanofluid past a permeable nonlinear shrinking sheet with heat source/sink.

Based on the observations from the above cited work, the purpose of present paper is to analyze the effect of second order slip and nonlinear thermal radiation and non-uniform heat source/sink on heat and momentum transfer of steady two-dimensional slip flow of a nanofluid over a stretching sheet. Governing nonlinear ordinary differential equations obtained after the application of similarity transformations are solved numerically by means of Runge-Kutta-Fehlberg-45 order method. The effects of different flow parameters on flow fields are elucidated through graphs and tables.

2. Mathematical formulation

Let us consider a steady flow of an incompressible Jeffrey nanofluid over a horizontal stretching surface. The flow region is confined to $y > 0$ and the plate is stretched along x-axis with a velocity $U_w = ax$, where a is a positive constant. A uniform magnetic field B_0 is applied in the transverse direction y normal to the plate. The nanofluid is assumed to be single phase, in thermal equilibrium and there is a slip velocity between the base fluid and particles. The stretching surface temperature and the nanoparticles fraction are deemed to have a constant value T_w and C_w, respectively. The ambient fluid temperature and nanoparticales fraction have constant value T_∞ and C_∞, respectively. The coordinate system and flow regime is illustrated as shown in the figure (1).
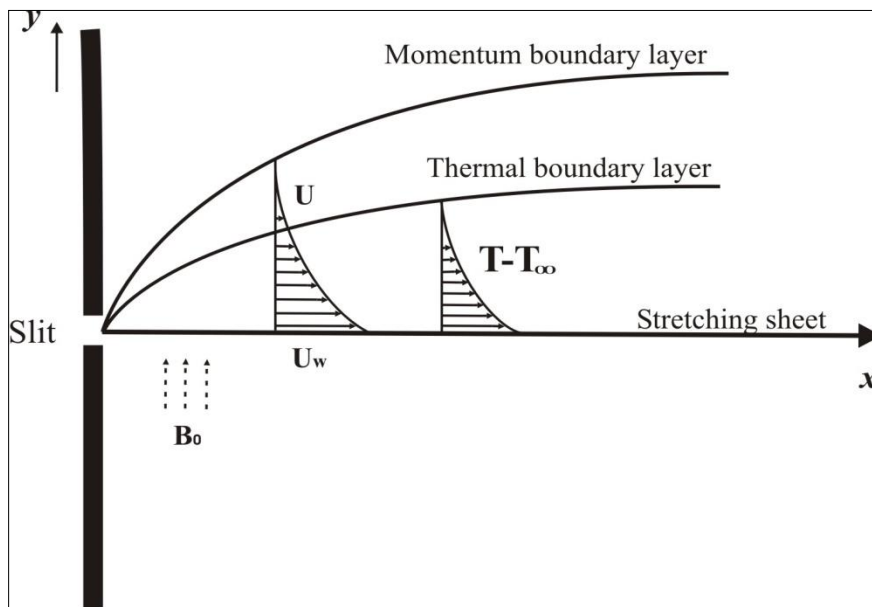
Figure 1 Physical model and coordinate system

It is well known that the constitutive equations for a Jeffrey fluid are given by Bilal Ashraf [24]

$$\tau = -pI + S,$$

$$S = \frac{\mu}{1+\lambda}\left[R_1 + \lambda_1\left(\frac{\partial R_1}{\partial t} + V.\nabla\right)R_1\right],$$

Where τ is the Cauchy stress tensor, S is the extra stress tensor, μ is the dynamic viscosity, λ and λ_1 are the material parameters of Jeffrey fluid and R_1 is the Rivlin–Ericksen tensor defined by

$$R_1 = (\nabla V) + (\nabla V)'.$$

Under usual boundary layer approximations governing two-dimensional equations for the present problem are given as:

$$\frac{\partial u}{\partial x} + \frac{\partial v}{\partial y} = 0, \qquad (1)$$

$$u\frac{\partial u}{\partial x} + v\frac{\partial u}{\partial y} = \frac{\nu}{1+\lambda}\left[\frac{\partial^2 u}{\partial y^2} + \lambda_1\left(u\frac{\partial^3 u}{\partial x \partial y^2} + v\frac{\partial^3 u}{\partial y^3} - \frac{\partial u}{\partial x}\frac{\partial^2 u}{\partial y^2} + \frac{\partial u}{\partial y}\frac{\partial^2 u}{\partial x \partial y}\right)\right] - \frac{\sigma B_0^2}{\rho_f}u, \quad (2)$$

$$u\frac{\partial T}{\partial x} + v\frac{\partial T}{\partial y} = \alpha\frac{\partial^2 T}{\partial y^2} + \frac{\rho_p c_p}{(\rho c)_f}\left[D_B\frac{\partial C}{\partial y}\frac{\partial T}{\partial y} + \frac{D_T}{D_\infty}\left(\frac{\partial T}{\partial y}\right)^2\right] - \frac{1}{(\rho c)_f}\frac{\partial q_r}{\partial y} + \frac{q'''}{(\rho c)_f}, \quad (3)$$

$$u\frac{\partial C}{\partial x} + v\frac{\partial C}{\partial y} = D_B\frac{\partial^2 C}{\partial y^2} + \frac{D_T}{D_\infty}\frac{\partial^2 T}{\partial y^2} - k_1(C - C_\infty). \qquad (4)$$

The corresponding boundary conditions are given by,

$$u = U_w + U_{slip}, \qquad v = 0, \qquad T = T_w, \qquad C = C_w \text{ at } y = 0,$$

$$u = 0, \ T = T_\infty, \ C = C_\infty, \ \text{as } y \to \infty, \qquad\qquad (5)$$

Where U_{slip} is the slip velocity at the surface and it is negative due to stretching. Wu's [25] slip velocity model used in this paper and is valid for arbitrary Knudsen numbers and is given as follows:

$$U_{slip} = \frac{2}{3}\left(\frac{3-\chi l^3}{\chi} - \frac{3}{2}\frac{1-l^2}{K_n}\right)\omega\frac{\partial u}{\partial y} = \frac{1}{4}\left[l^4 + \frac{2}{K^2_n}(1-l^2)\right]\omega^2\frac{\partial^2 u}{\partial y^2} = A\frac{\partial u}{\partial y} + B\frac{\partial^2 u}{\partial y^2} \quad (6)$$

Where $l = \min\left[\frac{1}{k_N}, 1\right]$, χ is the momentum accommodation coefficient with $0 \leq \chi \leq 1$, ω is the molecular mean free path, and K_n is the Knudsen number defined as the mean free path ω divided by a characteristic length for the flow. Based on the definition of l, it is seen that for any given value of K_n, we have $0 \leq l \leq 1$. The molecular mean free path is always positive. Thus we know that $B < 0$ and A is a positive number.

Here, q''' is the space and temperature dependent internal heat generation/absorption (non uniform heat source/sink) which can be expressed as,

$$q''' = \left(\frac{kU_w(x)}{xv}\right)[A^*(T_w - T_\infty)f'(\eta) + B^*(T - T_\infty)] \qquad (7)$$

Where T_w and T_∞ denote the temperature at the wall and at large distance from the wall respectively. A^* and B^* are the parameters of the space and temperature dependent internal heat generation/absorption. It is to be noted that A^* and B^* are positive to internal heat source and negative to internal heat sink.

Unlike the linearized Rosseland approximation, we use nonlinear Rosseland diffusion approximation from which one can obtain results for both small and large differences between T_w and T_∞. Using Rosseland [26] approximation for radiation, the radiative heat flux is simplified as,

$$q_r = -\frac{4\sigma^*}{3k^*}\frac{\partial T^4}{\partial y}. \qquad (8)$$

For a boundary layer flow over a horizontal flat plate (Pantokratoras and Fang [12]), from equation (8) we get,

$$q_r = \left(-\frac{16\sigma^* T_\infty^3}{3k^*}\right)\frac{dT}{dy}. \qquad (9)$$

In view to equation (9), energy equation (3) will becomes

$$u\frac{\partial T}{\partial x} + v\frac{\partial T}{\partial y} = \frac{\partial}{\partial y}\left[\left(\alpha + \frac{16\sigma^* T_\infty^3}{3k^*(\rho c)_f}\right)\frac{\partial T}{\partial y}\right] + \frac{\rho_p c_p}{(\rho c)_f}\left[D_B\frac{\partial C}{\partial y}\frac{\partial T}{\partial y} + \frac{D_T}{D_\infty}\left(\frac{\partial T}{\partial y}\right)^2\right] + \frac{q'''}{(\rho c)_f} \quad (10)$$

Where $\alpha = \frac{k}{(\rho c)_f}$, k being the thermal conductivity.

The governing equations can be reduced to ordinary differential equations, using the following similarity transformations,

$$u = axf'(\eta), \quad v = -\sqrt{av}f(\eta), \quad \eta = \sqrt{\frac{a}{v}}y,$$

$$T = T_\infty\big(1 + (\theta_w - 1)\theta(\eta)\big), \quad \phi(\eta) = \frac{C - C_\infty}{C_w - C_\infty}. \tag{11}$$

where $\theta_w = \frac{T_w}{T_\infty}$, $\theta_w > 1$, the temperature ratio parameter (Shehzad et al. [13]).

With the help of aforementioned transformations, equation (1) is identically satisfied and equations (2), (4) and (10) will take the following forms;

$$f''' + (1 + \lambda)[ff'' - f'^2] + \beta[f''^2 - ff''''] - (1 + \lambda)(M)f' = 0, \tag{12}$$

$$[1 + Nr\,(1 + (\theta_w - 1)\theta)^3\theta']' + \Pr[f\theta' + Nb\phi'\theta' + Nt(\theta')^2]$$

$$+ A^* f'(\eta) + B^* \theta(\eta) = 0, \tag{13}$$

$$\phi'' + Lef\phi' + \frac{Nt}{Nb}\theta'' - \gamma\phi = 0. \tag{14}$$

The corresponding boundary conditions are;

$$f(0) = 0, \ f'(0) = 1 + A_1 f''(0) + A_2 f'''(0), \ \theta(0) = 1, \ \phi(0) = 1 \ \text{at}\ \eta = 0,$$

$$f'(\eta) = f''(\eta) = \theta(\eta) = \phi(\eta) = 0 \ \text{as}\ \eta \to 0, \tag{15}$$

where, A_1 is the first-order velocity slip parameter with $0 < A_1 = A\sqrt{\frac{a}{\nu}}$ and A_2 is the second-order velocity slip parameter with $0 > A_2 = \frac{Ba}{\nu}$. Further, f, θ and ϕ are functions of η and prime denotes derivatives with respect to η. $\beta = a\lambda_1$ is Deborah number, $M = \frac{\sigma B_0^2}{\rho_f a}$ is magnetic parameter called Hartmann number, $Nr = \frac{16\sigma^* T^3_\infty}{3kk^*}$ is radiation parameter, $Nb = \frac{\tau D_B(C_w - C_\infty)}{\nu}$ is Brownian motion parameter, $Nt = \frac{\tau D_T(T_w - T_\infty)}{\nu T_\infty}$ is thermophoresis parameter, $Pr = \frac{\nu}{\alpha}$ is Prandtl number, $\gamma = \frac{k_1 Le}{a}$ is chemical reaction parameter, and $Le = \frac{\nu}{D_B}$ is Lewis number.

The skin friction coefficient (Cf_x), local Nusselt number (Nu_x) and Local Sherwood number (Sh_x) are given by,

$$Cf_x = \frac{\tau_w}{\rho U_w^2}, \ Nu_x = \frac{xq_w}{k(T_w - T_\infty)} \ \text{and}\ Sh_x = \frac{xq_m}{k(C_w - C_\infty)} \tag{16}$$

where the shear stress along the stretching surface τ_w, the surface heat flux q_w and the surface mass flux q_m are

$$\tau_w = \frac{\mu}{1 + \lambda}\left[\left(\frac{\partial u}{\partial y}\right) + \lambda_1\left(\frac{\partial^2 u}{\partial x \partial y} + u\frac{\partial^2 v}{\partial x^2} + v\frac{\partial^2 u}{\partial y^2}\right)\right]_{y=0},$$

$$q_w = -k\frac{\partial T}{\partial y} + (q_r)_w, \ q_m = -D_B\frac{\partial C}{\partial y} \ \text{at}\ y = 0. \tag{17}$$

Substituting the values of τ_w, q_w and q_m into the equation (16) we have

$$\sqrt{Re}\,Cf_x = \left[\frac{1}{1+\lambda}\big(f''(0) + \beta(f'(0)f''(0)) - f(0)f'''(0)\big)\right],$$

$$\frac{Nu_x}{\sqrt{Re_x}} = -(1 + Nr\theta^3{}_w)\theta'(0), \ \frac{Sh_x}{\sqrt{Re_x}} = -\phi'(0), \tag{18}$$

where $Re_x = \frac{ax^2}{\nu}$ is local Reynolds number.

2.1. Numerica method

The system of non-linear ordinary differential equations (12) to (14) with boundary conditions (15) has been solved using Runge-Kutta-Fehlberg fourth-fifth order method along with Shooting technique. The method has the following steps: In the first step, the governing system of equations (12) to (14) are reduced to a system of eight simultaneous differential equations of first order by introducing new dependent variables. In this system of first order differential equations, four initial conditions are known and remaining missed initial conditions are obtained with the help shooting technique. Afterward, a finite value for η_∞ is chosen in a such a way that all the far field boundary conditions are satisfied asymptotically. Our bulk computations are considered with the value at $\eta_\infty = 5$, which is sufficient to achieve the far field boundary conditions asymptotically for all values of the parameters considered. After fixing finite value for η_∞, integration is carried out with the help of Runge-Kutta-Fehlberg-45 (RKF-45) method. Runge-Kutta-Fehlberg-45 method has a procedure to determine if the proper step size h is being used. At each step, two different approximations for the solution are made and compared. If the two answers are in close agreement, the approximation is accepted otherwise, the step size is reduced until to get the required accuracy. For the present problem, we took step size $\Delta\eta = 0.001$, far field boundary conditions at $\eta_\infty = 5$ and accuracy to the fifth decimal places. To have a check on the accuracy of the numerical procedure used, first test computations for $\theta'(0)$ are carried out for viscous fluid for various values of Pr and compared with the available published results of Goyal and Bhargava [27], Gorla and Sidawi [28], Nadeem and Hussain [29] and Wang [30] in Table – (1) and they are found to be in excellent agreement.

3. Results and discussion

A theoretical investigation of second order velocity slip boundary layer flow of Jeffrey nanofluid over a stretching sheet under the influence of nonlinear thermal radiation and non-uniform heat source/sink has been performed. The value of the Prandtl number for the base fluid is kept as $Pr = 10$. The default values of the other parameters are mentioned in the description of the respected figures. In order to study the characteristics of velocity and temperature distribution for first order velocity slip parameter (A_1) and second order velocity slip parameter (A_2), radiation parameter (Nr), temperature ratio parameter (θ_w), magnetic parameter (M) graphs are platted and physical reasons behind the trend of the graphs are discussed.

The effect of first order and second order velocity slip parameters on velocity and temperature profiles are demonstrated as in the figure (2) and (3). We can observe that the effect of increasing values of both first and second order velocity slip parameters reduces the thickness of momentum boundary layer and hence decrease the velocity. Therefore, increasing values of velocity slip parameters (A_1 and A_2) decrease the boundary layer velocity, where as the temperature increases with increase in A_1 and A_2. This must be due to the existence of slip velocity on the stretching surface.
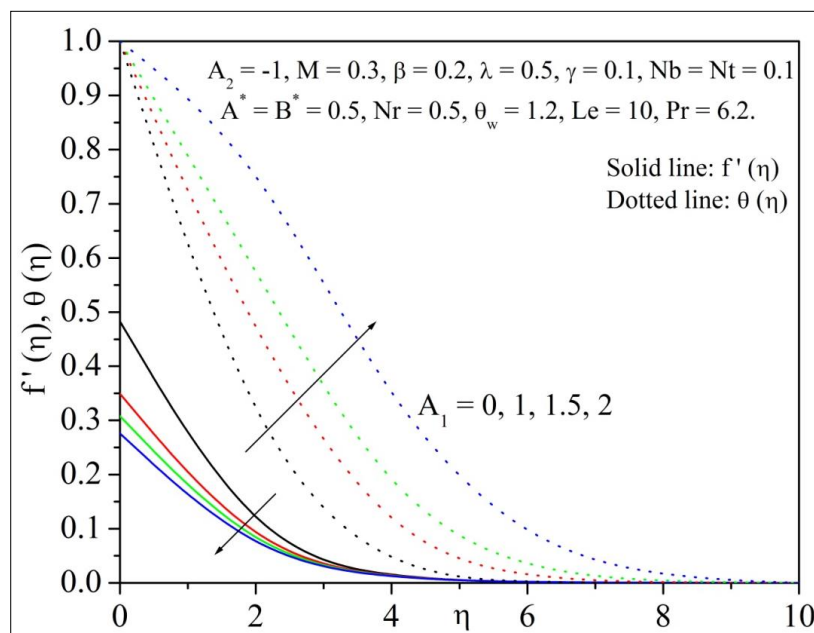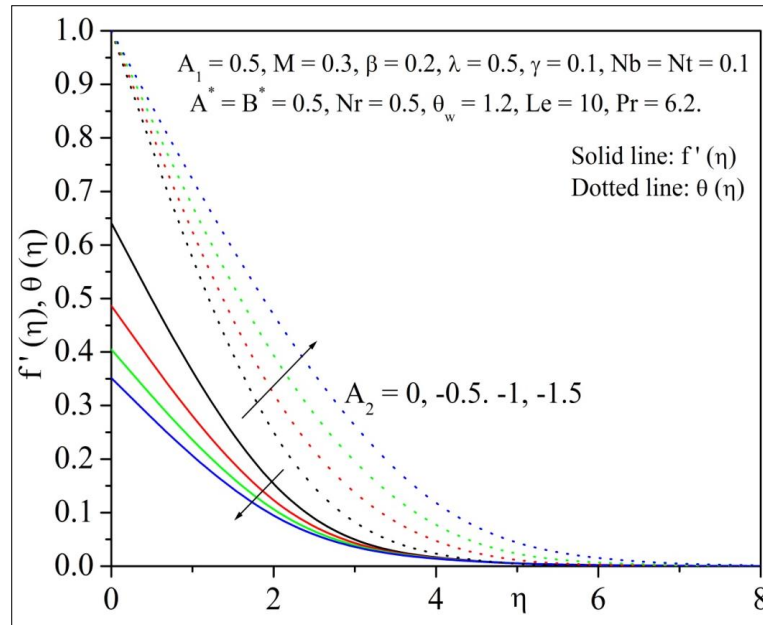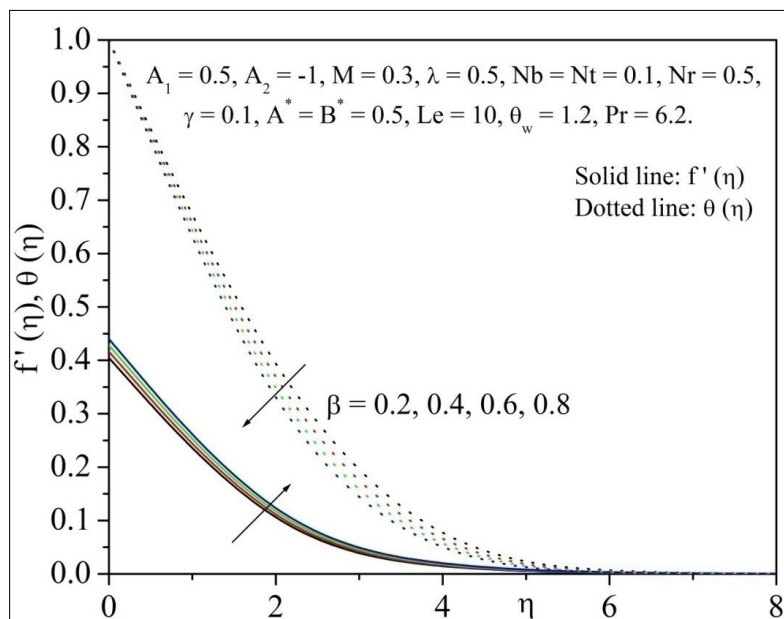

Figure 2 Velocity and temperature profile for various values of A_1.

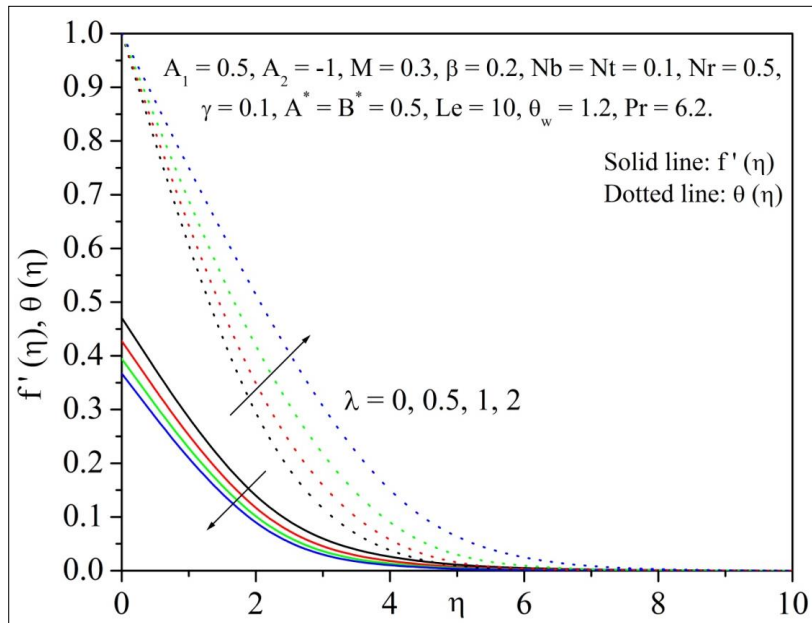**Figure 3** Velocity and temperature profile for various values of A_2.

Figure (4) describes the effects of Deborah number (β) on the velocity and temperature profiles. We can see that boundary layer thickness and the fluid velocity increases with increase in β. This is because; increase in β decreases the resistance of fluid motion which thus causes a higher fluid movement at the neighborhood of the stretching surface. Figure (4) reveals that the larger values of Deborah number leads to a reduction in the temperature and thermal boundary layer thickness. It is due to the fact that Deborah number is directly proportional to relaxation time and larger values of Deborah number corresponds to the higher relaxation time. Such increase in relaxation time corresponds to the lower temperature and weaker thermal boundary layer thickness. We can also see that boost in β causes the reduction in the concentration boundary layer.

Figure 4 Velocity and temperature profile for various values of β.

Influence of λ on velocity and temperature profile is highlighted in figure (5). It can be seen that an increase in λ decreases the fluid velocity but enhances the temperature profile and it gives rise to the nanoparticle concentration field and associated boundary layer thickness. It is due to the fact that an increase in λ corresponds to decrease in

retardation time but increase in the relaxation time and hence higher values of λ imply the domination of relaxation time over retardation time due to which temperature and concentration profiles are enhanced.

**Figure 5** Velocity and temperature profile for various values of λ.

Figure (6) shows the effect of magnetic parameter (M) on dimensionless velocity and temperature distributions, respectively. The presence of a magnetic field in an electrically conducting fluid induces a force called Lorentz force, which opposes the flow. This resistive force tends to slow down the flow, so the effect of M decreases the velocity and also cause increase in its temperature distributions.

Figure (7) depicts the temperature profiles for several values of A^*, it can be seen that the thermal boundary layer generates the energy and this causes the temperature profiles increases with increase in ($A^* > 0$) and decreases with increase in ($A^* < 0$).
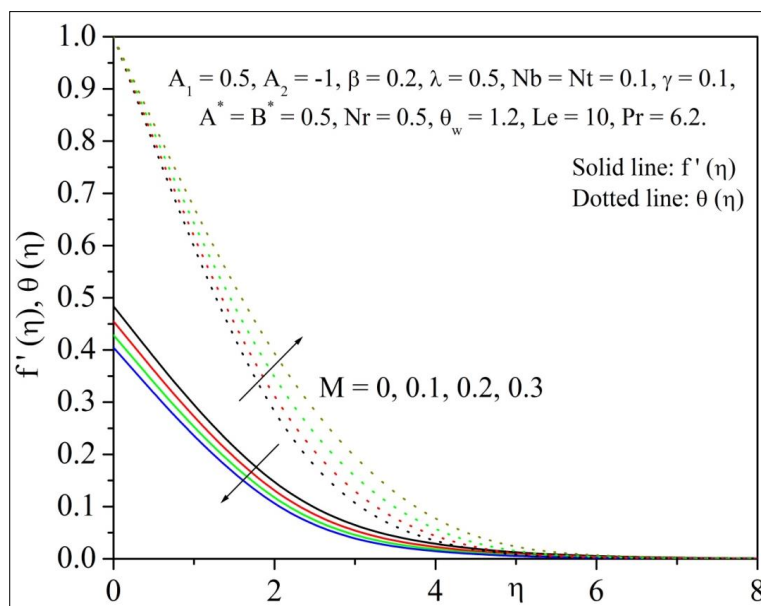
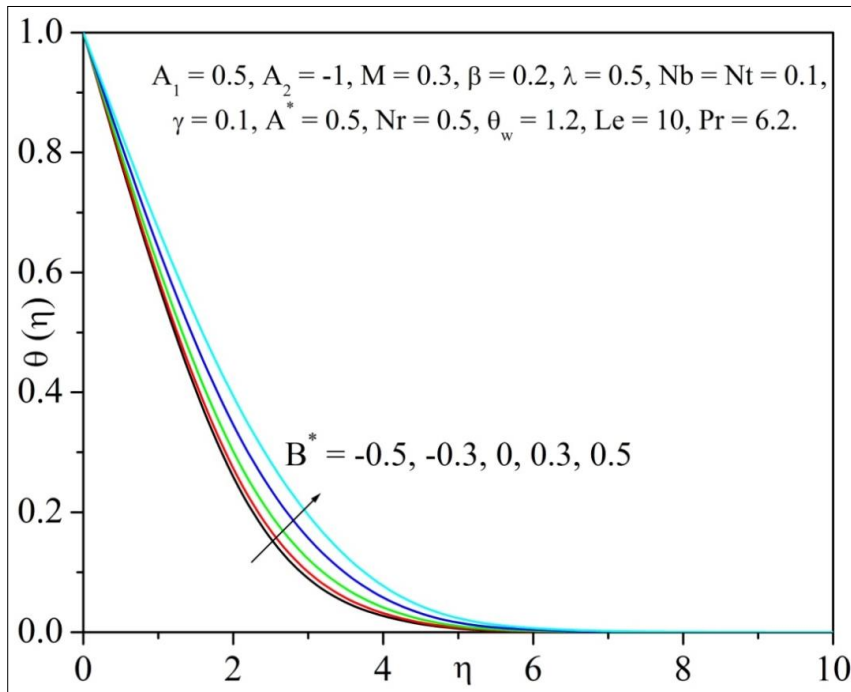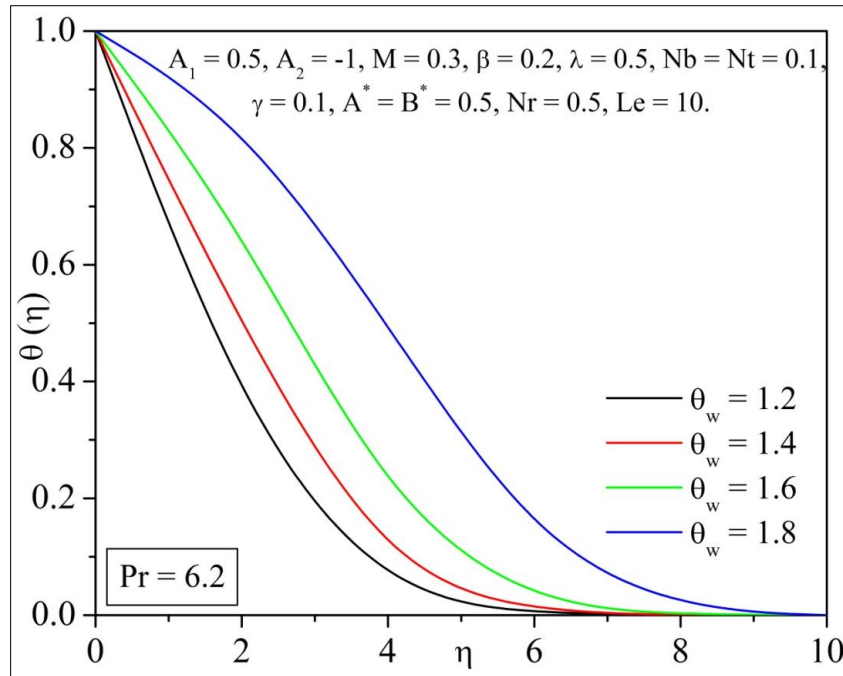**Figure 6** Velocity and temperature profile for various values of M.
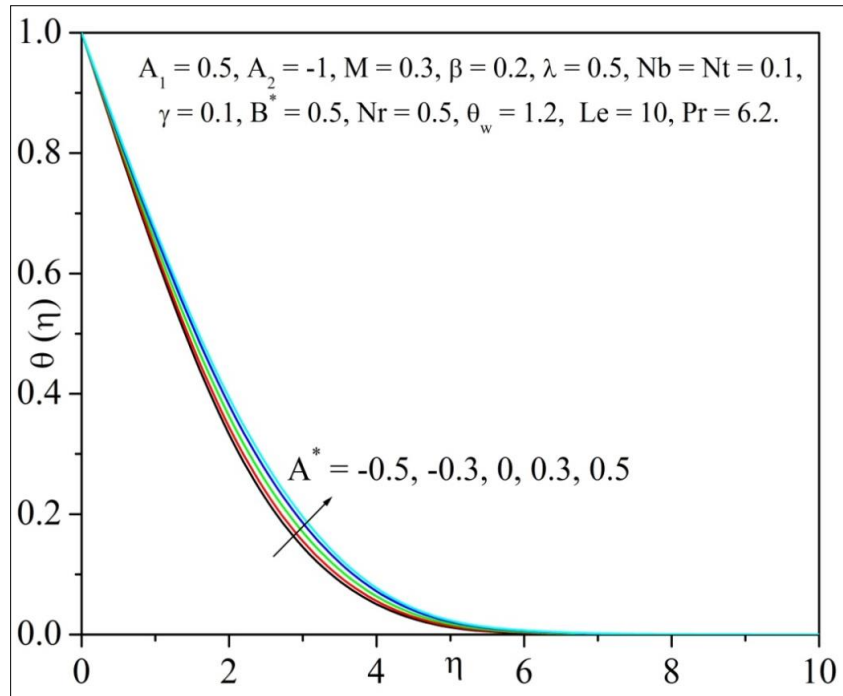
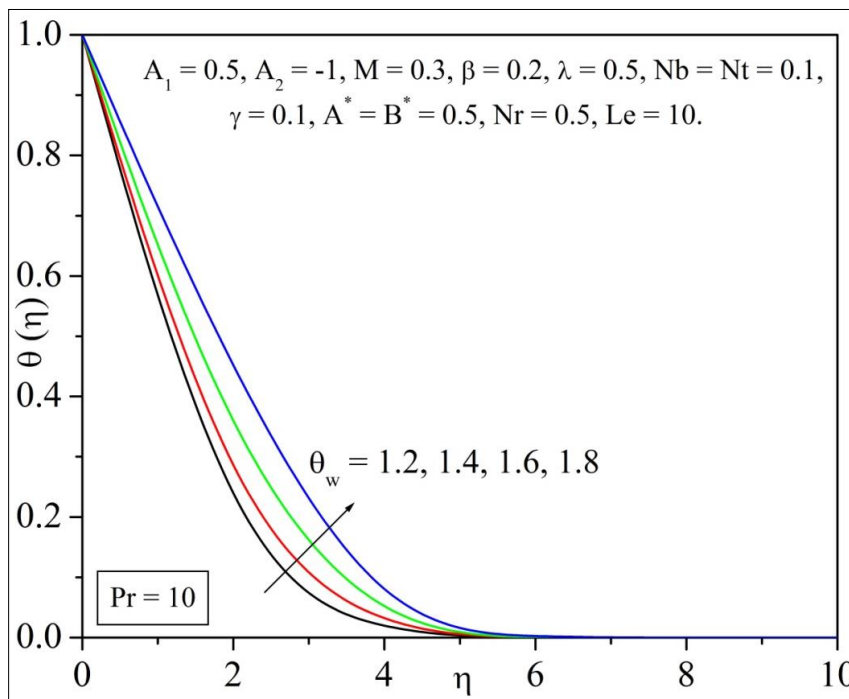**Figure 7** Temperature profile for various values of A^*.

Figure 8 Temperature profile for various values of B^*.

The effect of temperature dependent heat source/sink parameter (B^*) on temperature profile was demonstrated in figure (8). This graph illustrates that energy is released for increasing values of $(B^* > 0)$ which causes the temperature to increase, where as energy is absorbed for decreasing values of $(B^* < 0)$ resulting the temperature to drop significantly within the boundary layer.
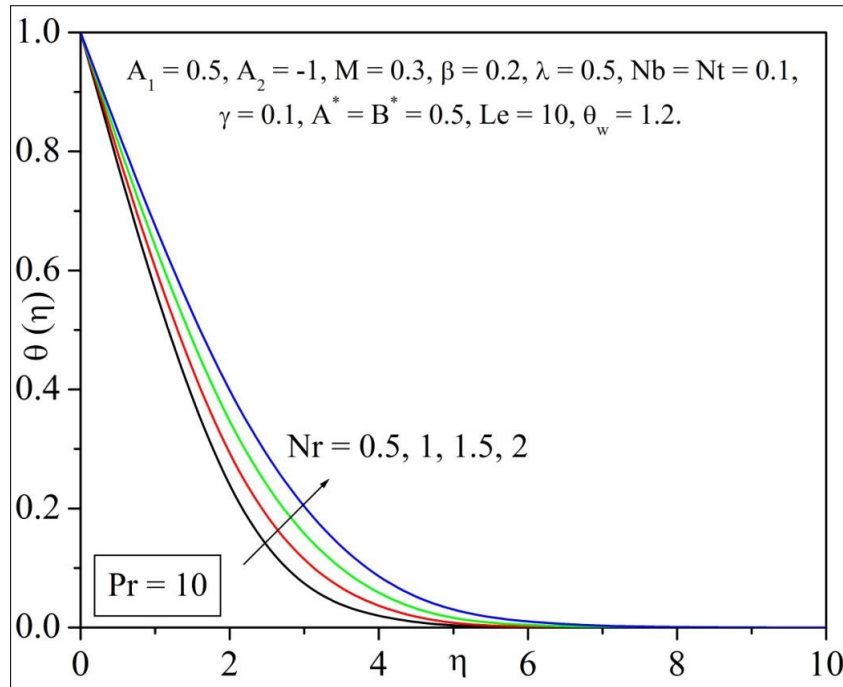
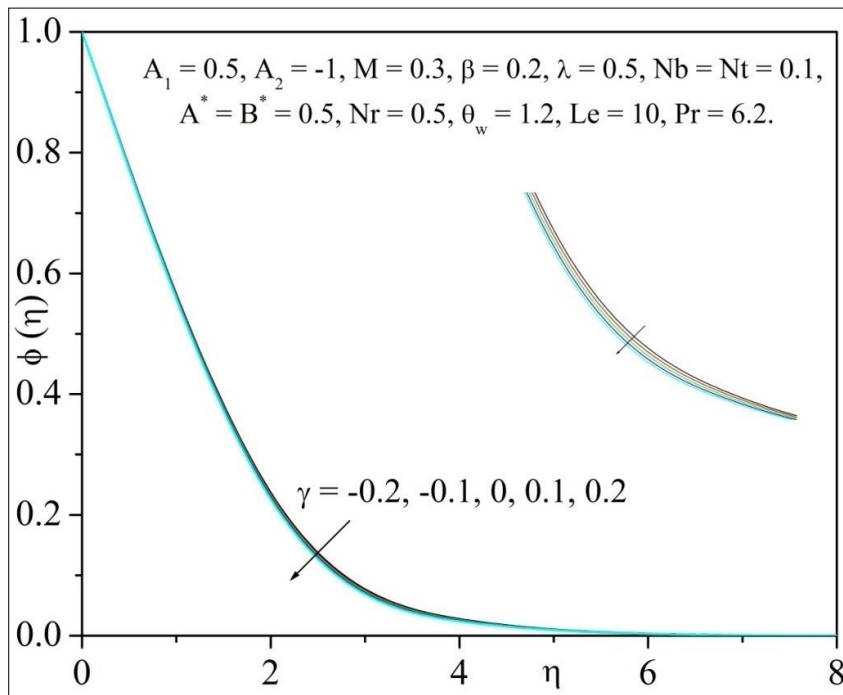**Figure 9** Temperature profile for various values of θ_w when $Pr = 6.2$.

Figure 10 Temperature profile for various values of θ_w when $Pr = 10$.

Figure (9) and (10) illustrates the effect of temperature ratio parameter (θ_w) on temperature profiles, when $Pr = 6.2$ and $Pr = 10$ respectively. From these plots, one can notice that, an increase in temperature ratio parameter increases the thermal state of the fluid, and it results in increase of temperature profiles. The effect of radiation parameter on temperature is depicted as in figure (11). A critical observation shows that, the temperature profile increases with increase in Nr. This is because; an increase in the radiation parameter provides more heat to fluid that causes an enhancement in the temperature and thermal boundary layer thickness.

Figure 11 Temperature profile for various values of *Nr*.

Figure 12 Nanoparticle concentration profile for various values of γ.
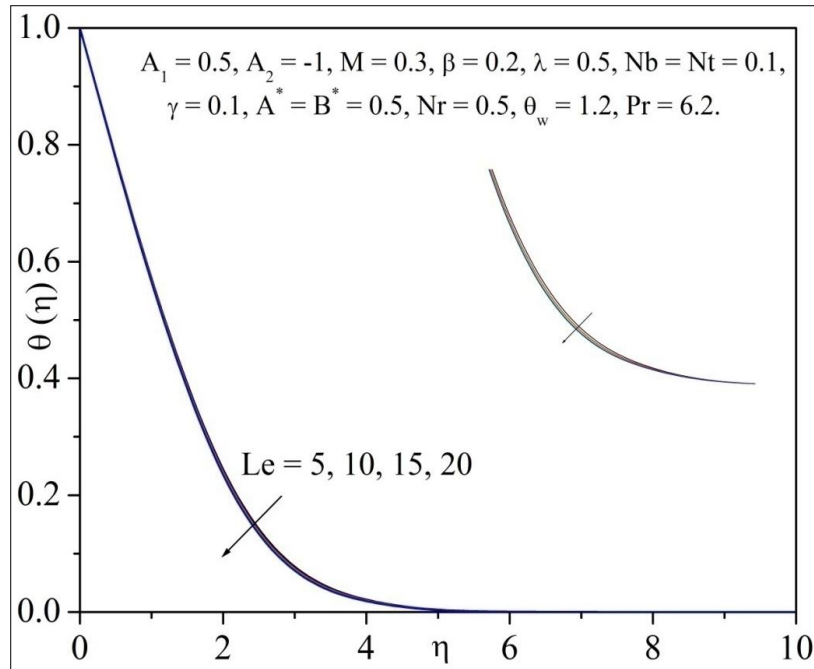
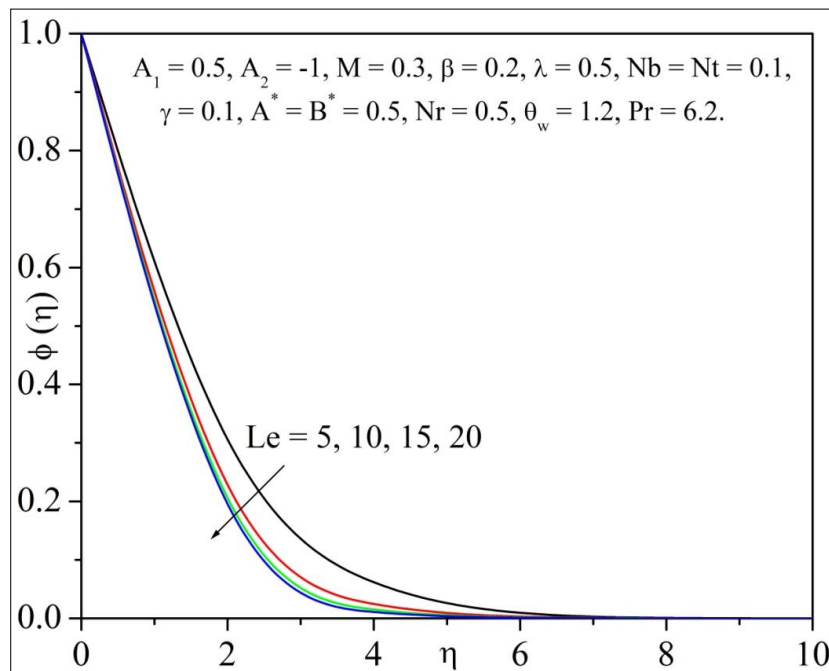**Figure 13** Temperature profile for various values of *Le*.

Figure 14 Nanoparticle concentration profile for various values of *Le*.

Effect of chemical reaction parameter (γ) on nanoparticle volume fraction profile is shown in figure (12) for the both negative and positive values of γ. It is observed that the nanoparticle volume fraction decreases for constructive chemical reaction parameter and increases for destructive chemical reaction parameter.

Figure (13) and (14) displays the effect of Lewis number (Le) on temperature and concentration profiles. From these figures both the profiles decreases with increasing values of Le. It is due to the fact that the larger values of Lewis number make the mass diffusivity smaller; therefore it decreases the concentration field.

Temperature and nanoparticle volume fraction variation against different values of Nb and Nt are depicted respectively, as in figure (15), (16) and (17). We can see that the temperature profiles are increasing function of Nb,

whereas nanoparticle volume fraction is a decreasing one. This may be due to the fact that as Brownian motion parameter (Nb) decreases the mass transfer of a nanofluid. Further, both temperature and nanoparticle volume fraction profiles increases for increasing values of Nt. The variation in Prandtl number (Pr)on θ (for $A^* = B^* = 0.1$) is shown in figure (18). The temperature field (θ) decreases when Pr increases. It is obvious that, an increase in the values of Pr reduces the thermal diffusivity, therefore thermal boundary layer thickness is a decreasing function of Pr.

Figure 15 Temperature and Nanoparticle concentration profile for various values of $\boldsymbol{Nb}$.
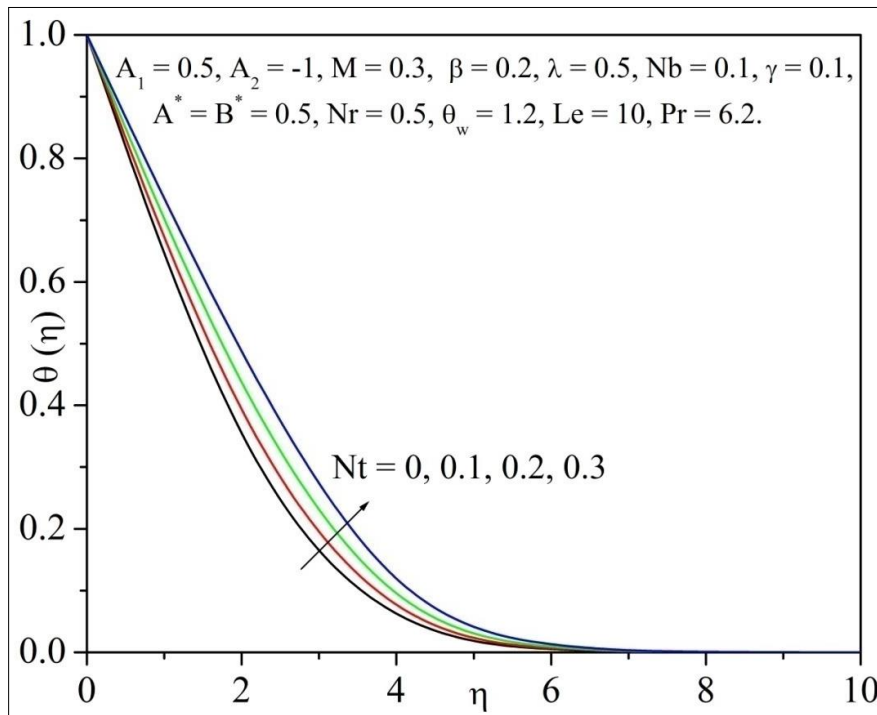
Figure 16 Temperature profile for various values of $\boldsymbol{Nt}$.
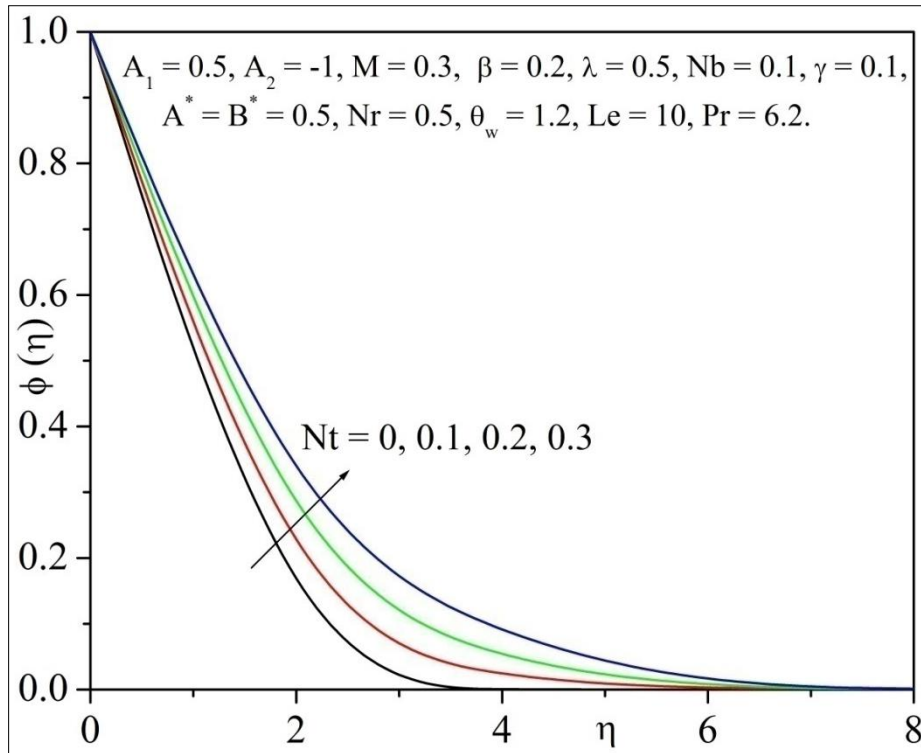
Figure 17 Nanoparticle concentration profile for various values of Nt.

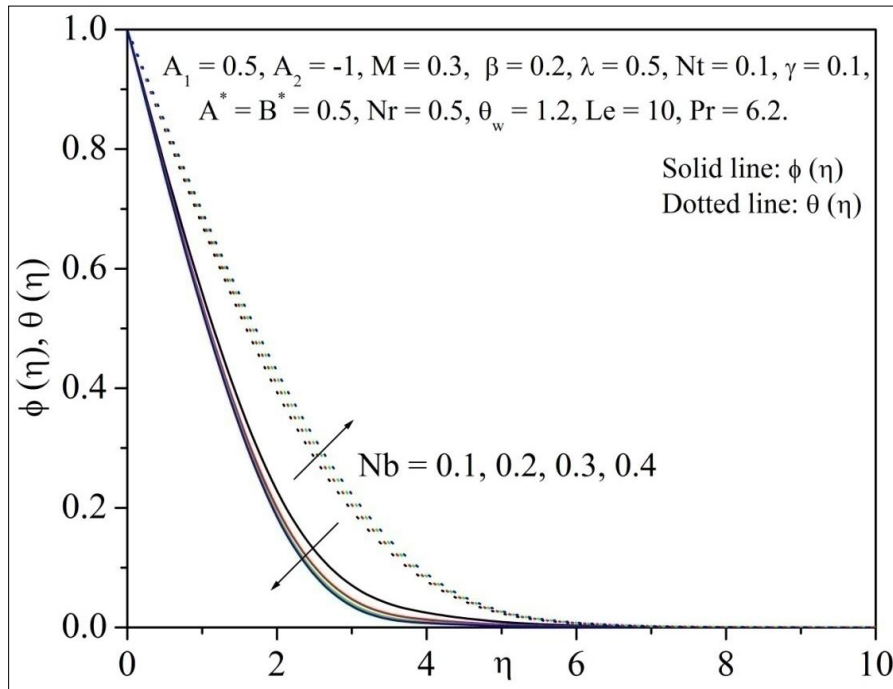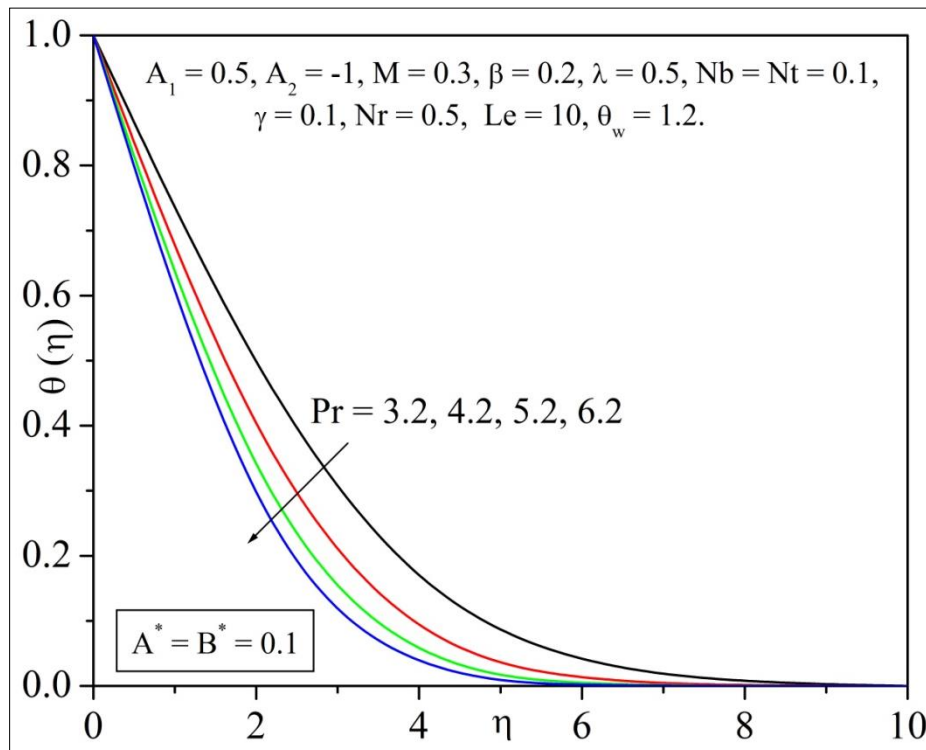

Figure 18 Temperature profile for various values of Pr when $A^* = B^* = 0.1$.

The numerical results recorded in Table – (2) illustrates the variation of skin friction co-efficient and Nusselt number with respect to various flow controlling parameters. As expected, both first and second order velocity slip parameters effect is to reduce the friction at the solid-fluid interface, and thus reduces the skin friction coefficient. Similar behaviour is also observed in the case of λ, i.e., in the presence velocity slip, increase in λ results decrease of both skin friction coefficient and local Nusselt number. But quite opposite behaviour is observed in the case of β and M.

The effects of various pertinent parameters on local Nusselt number and local Sherwood number are discussed numerically through Table – (3). We can see that A^*, B^*, γ, Le and Pr shows favourable effect on coefficient of $\phi'(0)$, whereas effect of θ_w, Nb and Nt on local Nusselt number is negligible. We can also observe that both θ_w and Pr show positive effect on local Nusselt number. This is due to the fact that a higher Prandtl number reduces the thermal boundary layer thickness and increases the surface heat transfer rate. Also high Prandtl number implies more viscous fluid which tends to retard the motion. Similarly, A^*, B^*, θ_w shows negative effect and chemical parameter has no effect on local Nusselt number.

Table 1 Comparison table for $-\theta'(0)$ (viscous case) with $\beta = \lambda = A_1 = A_2 = Nr = A^* = B^* = \gamma = 0, Nb = Nt = 10^{-6}$

Pr	Nadeem and Hussain (HAM method) (2013)	Gorla and Sidawi (1994)	Goyal and Bhargava (FEM Method) (2014)	Wang (1989)	Present (RKF45 Method)
0.2	0.169	0.1691	0.1691	0.1691	0.170259788
0.7	0.454	0.5349	0.4539	0.4539	0.454447258
2	0.911	0.9114	0.9113	0.9114	0.911352755
7		1.8905	1.8954	1.8954	1.895400395
20		3.3539	3.3539	3.3539	3.353901838

Table 2 Values of Skin friction coefficient and Nusselt number for different values of the parameters when $Pr = 6.2, \theta_w = 1.2, Nr = 0.5, A^* = B^* = 0.5$.

A_1	A_2	β	λ	M	$-\sqrt{Re}Cf_x$	$-\dfrac{Nu_x}{\sqrt{Re_x}}$
0					0.3650	0.4217
1					0.2380	0.1771
1.5					0.2020	0.0403
	0				0.5400	0.6069
	-0.5				0.3690	0.4266
	-1				0.2880	0.2973
		0.2			0.2880	0.2973
		0.4			0.3110	0.3360
		0.6			0.3350	0.3702
			0		0.4320	0.4736
			0.3		0.3330	0.3687
			0.6		0.2700	0.2598
				0	0.2880	0.5004
				0.1	0.2890	0.4375
				0.2	0.2890	0.3708

Table 3 Values of Nusselt and Sherwood number for different values of the parameters when $A_1 = 0.5, A_2 = -1, \beta = 0.2, \lambda = 0.5, M = 0.3$.

A^*	B^*	Nr	θ_w	Nb	Nt	γ	Le	Pr	$-\dfrac{Sh_x}{\sqrt{Re_x}}$	$-\dfrac{Nu_x}{\sqrt{Re_x}}$
-0.5									1.3796	0.5296
0									1.4154	0.4145
0.5									1.4521	0.2973
	-0.5								1.2618	0.9041
	0								1.3441	0.6537
	0.5								1.4521	0.2973
		0.5							1.4502	0.2973
		1							1.4521	0.3246
		1.5							1.4558	0.2691
			1.2						1.4521	0.2973
			1.4						1.4520	0.2642
			1.6						1.4510	0.1956
				0.1					1.4540	0.2973
				0.2					1.4521	0.2066
				0.3					1.4520	0.1350
					0				1.4250	0.3916
					0.1				1.4521	0.2973
					0.2				1.5174	0.2113
						-0.2			1.3169	0.2971
						-0.1			1.3639	0.2970
						0			1.4089	0.2972
						0.1			1.4521	0.2973
						0.2			1.4936	0.2975
							5		0.9829	0.3001
							10		1.4521	0.3000
							20		2.1209	0.2973
								4.2	1.3598	0.5251
								5.2	1.3471	0.6073
								6.2	1.3380	0.6705

Nomenclature

- a stretching rate
- A^* space dependent heat source/sink
- A_1 the first-order velocity slip parameter
- A_2 the second-order velocity slip parameter

- B^* temperature dependent heat source/sink
- B_0 magnetic field strength
- C volumetric volume expansion coefficient
- Cf_x local skin friction coefficient
- D_B Brownian diffusion coefficient
- D_T thermophoresis diffusion coefficient
- k_1 chemical reaction coefficient
- k thermal conductivity
- k^* Rosseland mean absorption coefficient
- Le Lewis number
- M magnetic parameter
- Nb Brownian motion parameter
- Nr radiation parameter
- Nt thermophoresis parameter
- Nu_x local Nusselt number
- Pr Prandtl number
- Re_x local Reynolds number
- Sh_x local Sherwood number
- T temperature of the nanofluid near wall
- T_∞ fluid temperature far away from the sheet
- T_w uniform wall temperature
- U_w stretching velocity
- u, v velocity components along the x and y axes

Greek symbols

- λ, λ_1 ratio of relaxation and retardation times and the relaxation time
- ρ_f density of the fluid
- ρ_p nanoparticles density
- θ dimensionless temperature variable
- ϕ nanoparticle volume fraction
- α thermal diffusivity
- η similarity variable
- v kinematic viscosity
- σ^* Stefan-Boltzmann constant
- $(\rho c)_f$ heat capacities of nanofluid
- $(\rho c)_p$ effective heat capacity of the nanoparticles
- β Deborah number
- γ chemical reaction parameter

Subscripts

- ∞ infinity
- w sheet surface

---

4. Conclusions

An analysis to study the effect of nonlinear thermal radiation on second order slip flow and heat transfer of Jeffrey nanofluid over a stretching sheet with non-uniform heat source/sink is presented. Numerical results for velocity profiles, surface heat transfer rate and mass transfer rate have been obtained for parametric variations of various ranges

of slip boundary condition and for different values of flow pertinent parameters. The main outcomes of the problem are summarized as follow;

- Both first and second order velocity slip parameter reduces the thickness of momentum boundary layer and hence decrease the velocity.
- Boundary layer thickness and the fluid velocity increases with increase in Deborah number.
- An increase in Lewis and Prandtl numbers shows a decrease in nanoparticle concentration.
- Larger values of magnetic parameter lead to an enhancement in the temperature and nanoparticle concentration.
- An increase in λ and θ_w enhances the temperature profile.
- Nanoparticle volume fraction decreases for constructive chemical reaction parameter and increases for destructive chemical reaction parameter.
- Both temperature and nanoparticle volume fraction increase for increasing values of Nr.
- Nr enhances the coefficient of Nusselt number, but the parameters θ_w, Nb, Nt decreases $-\theta'(0)$.

Compliance with ethical standards

Disclosure of conflict of interest

No competing interests.

Statement of informed consent

Informed consent was obtained from all individual participants included in the study.

References

[1] Fang, T., Yao, S., Zhang, J and Aziz, A. 2010a. Viscous flow over a shrinking sheet with a second order slip flow model". Commun. Nonlinear Sci. Numer. Simul. 15, 1831–1842.

[2] Fang, T and Aziz, A. 2010b. Viscous flow with second-order slip velocity over a stretching sheet. Z. Naturforsch. A – Phys. Sci. 65a, 1087–1092.

[3] Mahantesh, Nandeppanavar, M., Vajravelu, K., Subhas Abel, M and Siddalingappa, M.N. 2012. Second order slip flow and heat transfer over a stretching sheet with non-linear Navier boundary condition. International Journal of Thermal Sciences, 58, 143-150.

[4] Rosca, Natalia. C and Ioan Pop. 2013a. Mixed convection stagnation point flow past a vertical flat plate with a second order slip: Heat flux case. International Journal of Heat and Mass Transfer, 65, 102–109.

[5] Rosca, Alin. V and Ioan Pop. 2013b. Flow and heat transfer over a vertical permeable stretching/shrinking sheet with a second order slip. International Journal of Heat and Mass Transfer, 60, 355–364.

[6] Khader, M.M. 2014. Laguerre collocation method for the flow and heat transfer due to a permeable stretching surface embedded in a porous medium with a second order slip and viscous dissipation. Applied Mathematics and Computation, 243, 503–513.

[7] Abdul Hakeem, A.K., Vishnu Ganesh, N and Ganga, B. 2015. Magnetic field effects on second order slip flow of nanofluid over a stretching/shrinking sheet with thermal radiation effect". Journal of Magnetism and Magnetic Materials, 381, 243–257.

[8] Mabood Fazle, Mastroberardino Antonio. 2015. Melting heat transfer on MHD convective flow of a nanofluid over a stretching sheet with viscous dissipation and second order slip. Journal of the Taiwan Institute of Chemical Engineers, 1–7.

[9] Hayat, T., Taseer Muhammad, Alsaedi, A and Alhuthali, M.S. 2015b. Magnetohydrodynamic three-dimensional flow of viscoelastic nanofluid in the presence of nonlinear thermal radiation. Journal of Magnetism and Magnetic Materials, 385, 222–229.

[10] Zhu J, Liu Zheng, Liancun Zheng and Xinxin Zhang. 2015. Second-order slip MHD flow and heat transfer of nanofluids with thermal radiation and chemical reaction. Applied Mathematics and Mechanics, 36, (9), 1131-1146.

[11] Megahed, A. M. 2015. MHD viscous Casson fluid flow and heat transfer with second-order slip velocity and thermal slip over a permeable stretching sheet in the presence of internal heat generation/absorption and thermal radiation. The European Physical Journal Plus, 130, 81.

[12] Pantokratoras, A and Fang, T. 2013. Sakiadis flow with nonlinear Rosseland thermal radiation. Physica Scripta, 87, 015703.

[13] Shehzad Sabir Ali, Tasawar Hayat, Ahmed Alsaedi, Mustafa Ali Obid. 2014. Nonlinear thermal radiation in three-dimensional flow of Jeffrey nanofluid: A model for solar energy. Applied Mathematics and Computation, 248, 273–286.

[14] Hayat, T., Muhammad, T., Shehzad, S and Alsaedi, A. 2015d. Three-Dimensional Flow of Jeffrey Nanofluid with a New Mass Flux Condition. J. Aerosp. Eng., 0.1061/(ASCE)AS.1943-5525.0000549 , 04015054.

[15] Shehzad, S.A., Hayat, T and Alsaedi, A. 2015a. MHD flow of Jeffrey nanofluid with convective boundary conditions. Journal of the Brazilian Society of Mechanical Sciences and Engineering, 37(3), pp 873-883.

[16] Shehzad, S.A., Abdullah, Z., Alsaedi, A., Abbasi, F.M and Hayat, T. 2015b. Thermally radiative three-dimensional flow of Jeffrey nanofluid with internal heat generation and magnetic field. Journal of Magnetism and Magnetic Materials, 397, 108–114.

[17] Dalira Nemat, Mohammad Dehsara and Salman Nourazar, S. 2015. Entropy analysis for magnetohydrodynamic flow and heat transfer of a Jeffrey nanofluid over a stretching sheet. Energy, 79, 351–362.

[18] Abbasi, F.M., Shehzad, S.A., Hayat, T., Alsaedi, A and Mustafa A. Obid. 2015. Influence of heat and mass flux conditions in hydromagnetic flow of Jeffrey nanofluid. AIP Advances, 5, 037111 doi: 10.1063/1.4914549.

[19] Pal, D. 2011. Combined effects of non-uniform heat source/sink and thermal radiation on heat transfer over an unsteady stretching permeable surface. Commun. Nonlinear Sci. Numer. Simulat., 16, 1890–1904.

[20] Hakeem Abdul, A.K., Vishnu Ganesh, N and Ganga B. 2014. Effect of heat radiation in a Walter's liquid B fluid over a stretching sheet with non-uniform heat source/sink and elastic deformation. Journal of King Saud University – Engineering Sciences, 26, 168–175.

[21] Manjunatha, P.T., Gireesha, B.J and Prasannakumara, B.C. 2014. Thermal analysis of conducting dusty fluid flow in a porous medium over a stretching cylinder in the presence of non-uniform source/sink. International Journal of Mechanical and Materials Engineering, 1, 13.

[22] Pal, D and Chatterjee, S. 2015. Effects of radiation on Darcy-Forchheimer convective flow over a stretching sheet in a micropolar fluid with non-uniform heat source/sink. Journal of Applied Fluid Mechanics, 8(2), 207-212.

[23] Dhanai Ruchika, Puneet Rana and Lokendra Kumar. (2015). Critical values in slip flow and heat transfer analysis of non-Newtonian nanofluid utilizing heat source/sink and variable magnetic field: Multiple solutions. Journal of the Taiwan Institute of Chemical Engineers, http://dx.doi.org/10.1016/j.jtice.2015.06.026.

[24] Bilal Ashraf, M., Hayat, T., Alsaedi, A and Shehzad, S.A. 2015. Convective heat and mass transfer in MHD mixed convection flow of Jeffrey nanofluid over a radially stretching surface with thermal radiation. J. Cent. South Univ., 22, 1114–1123.

[25] Wu, L. 2008. A slip model for rarefied gas flows at arbitrary Knudsen number, Appl. Phys. Lett., 93, 253-103.

[26] Rosseland, S. 1931. Astrophysik und atom-theoretischeGrundlagen. Berlin: Springer.

[27] Goyal Mania and Bhargava Rama. 2014. Boundary layer flow and heat transfer of viscoelastic nanofluids past a stretching sheet with partial slip conditions. Appl. Nanosci., 4(6), 761-767.

[28] Gorla, R.S.R, Sidawi, I. 1994. Free convection on a vertical stretching surface with suction and blowing. Appl. Sci. Res., 52, 247–257.

[29] Nadeem, S and Hussain, S.T. 2013. Flow and heat transfer analysis of Williamson nanofluid. Appl. Nanosci., 4(8), 1005-1012.

[30] Wang, C.Y. 1989. Free convection on a vertical stretching surface. J. Appl. Math. Mech., 69, 418–420.